

## Supplemental Material

### **Ancient roots of tungsten in western North America**

**V. Elongo<sup>1</sup>, P. Lecumberri-Sanchez<sup>1\*</sup>, H. Falck<sup>2</sup>, K. Rasmussen<sup>1</sup>, L.J. Robbins<sup>3</sup>, R. Creaser<sup>1</sup>, Y. Luo<sup>1</sup>, D.G. Pearson<sup>1</sup>, C. Sarkar<sup>1</sup>, E. Adlakha<sup>4</sup>, M.C. Palmer<sup>5</sup>, J.M. Scott<sup>5</sup>, K. Hickey<sup>6</sup>, K. Konhauser<sup>1</sup>**

<sup>1</sup>*Department of Earth and Atmospheric Sciences, University of Alberta; Edmonton, Canada.*

<sup>2</sup>*Northwest Territories Geological Survey, Yellowknife, Canada.*

<sup>3</sup>*Department of Geology, University of Regina; Regina, Canada.*

<sup>4</sup>*Department of Geology, Saint Mary's University; Halifax, Canada.*

<sup>5</sup>*Department of Geology, University of Otago; Otago, New Zealand.*

<sup>6</sup>*Department of Earth, Ocean and Atmospheric Sciences, University of British Columbia, Vancouver, Canada.*

\*Corresponding author. Email: [lecumber@ualberta.ca](mailto:lecumber@ualberta.ca)

#### **This file includes:**

- Appendix S1: Detailed geology of the Cantung and Mactung deposits
- Appendix S2: Materials
- Appendix S3: Methods
- Appendix S4: Supplementary Figure 1 and details for data presented in figures

#### **Other Supplemental Materials for this manuscript include the following:**

- Online Resource 1 (Data presented in Figure 3 and in Supplementary Figure S1)
- Online Resource 2 (Data presented in Figure 4)

#### **□ APPENDIX S1: DETAILED GEOLOGY OF THE CANTUNG AND MACTUNG DEPOSITS**

Cantung and Mactung are two tungsten skarn deposits located in the eastern part of the Selwyn Basin close to the Yukon–Northwest Territories border. Cantung and Mactung show similar mineralogy and paragenetic evolution (Elongo et al., 2020). The mineralogy in the two deposits consists of a prograde skarn stage evolving from garnet-pyroxene to pyroxene facies; and an overprinting retrograde alteration stage evolving from the amphibole-rich facies to the biotite-rich facies (Elongo et al., 2020). These main stages

are further overprinted by a sulfide stage followed by late quartz-sulfides veins. Scheelite is the main tungsten-bearing mineral and is either disseminated in the different facies or present in quartz and/or sulfides veins.

### ➤ **The Cantung deposit**

The Cantung skarn deposit in the Northwest Territories is hosted in Upper Proterozoic to Upper Ordovician sedimentary rocks (Blusson, 1968). Four main sedimentary units from latest Precambrian to lower Cambrian age are present at Cantung: the “Lower Argillite” of the Narchilla/Vampire formation, and the “Swiss-Cheese” Limestone, the “Ore” Limestone, and “Upper Argillite” of the Sekwi formation. The sedimentary sequence is folded into a recumbent anticline and was intruded by the Mine Stock pluton, a monzogranite (Mathieson and Clark, 1984) belonging to the Tungsten suite. The Mine Stock ( $98.2 \pm 0.4$  Ma from U-Pb in zircon; Rasmussen, 2013) is associated with contact metamorphism of the sedimentary sequence hosting the Cantung skarn (Mathieson and Clark, 1984). Dykes locally crosscutting the Mine Stock pluton consist of fine-grained monzogranite, aplitic to porphyry alkali feldspar granite, and kersantitic lamprophyres (Mathieson and Clark, 1984).

The magmatic Mine Stock pluton is unlikely to be responsible for tungsten mineralization at Cantung. Despite its proximity to mineralization at Cantung, the Mine Stock pluton shows only local evidence of hydrothermal alteration (Mathieson and Clark, 1984) or fluid saturation. In contrast, dikes crosscutting the pluton are extensively altered suggesting that they could be associated with the fluid source or a fluid conduit. Furthermore, there is no evidence for extensive magmatic fractionation in the Mine Stock monzogranite, which is a common characteristic of magmatic sources for tungsten mineralization (Rasmussen et al., 2011). However, mineralization at Cantung ranges in age from ~103 to 96 Ma (Lentz, 2020), so while the upper portions of the Mine Stock pluton may not be the source of fluids and tungsten, magma, fluid and metals were likely derived from the same unexposed magma body at depth (Rasmussen et al., 2011).

### ➤ **The Mactung deposit**

The Mactung skarn deposit in Yukon is hosted in an isoclinally folded succession of sedimentary units ranging in age from latest Precambrian to late Ordovician (Dick and Hodgson, 1982). From older to younger, these units correspond to the Vampire formation (locally unit 1), Sekwi formation (locally unit 2B), Hess River formation (locally unit 3C), the Rabbitkettle formation (locally units 3D, 3E, 3F, 3G and 3H) and the Duo Lake

formation (locally unit 4 ; Gebru, 2017 ; Fischer et al., 2018). Tungsten mineralization at Mactung occurs in two exoskarn orebodies hosted in the carbonate rich units within Sekwi and Rabbitkettle formations (locally units 2B, 3D, 3E and 3F ; Dick and Hodgson, 1982; Gebru, 2017; Fischer et al., 2018).

Two biotite quartz monzonite plutons (and related porphyritic, aplitic and pegmatitic dykes) belonging to the Tungsten suite are spatially associated with the Mactung deposit: the Cirque Lake Stock (also called Mactung North Pluton) and the Rockslide Mountain Stock (also called Mactung South Pluton ; Atkinson and Baker, 1986 ; Gebru, 2017). The Cirque Lake Stock was originally proposed as the source of the mineralizing fluids because of its close spatial association with the Mactung mineralization. However, like at Cantung, the causal relationship between the pluton and the mineralization was challenged because of the lack of mineralization in the carbonate units at the contact with the pluton, the weak hydrothermal alteration around the pluton, and the lack of correlation between veining and alteration in the pluton and mineralized locations (Atkinson and Baker, 1986). Recent studies have shown that the skarn mineralization ( $97.5 \pm 0.5$  Ma from Re–Os in molybdenite, Selby et al., 2003) is broadly coeval with the crystallization of the Cirque Lake Stock and the Rockslide Mountain Stock ( $97.6 \pm 0.2$  Ma from U–Pb in zircon, Gebru, 2017). As at Cantung, the timing of the exposed granitic plutons and skarn mineralization overlap closely.

## □ APPENDIX S2: SAMPLING

Whole rock samples representative of the local lithologies at Cantung and Mactung were selected to determine their Samarium-Neodymium isotope composition. Whole rock samples from Cantung include two granitoids samples (Mine Stock pluton), one sample of aplitic dyke, one sample of lamprophyre dyke, one non-skarnified limestone sample (Swiss-Cheese Limestone), and two argillite samples (Lower Argillite and Upper Argillite). Whole rock samples from Mactung include two granitoids samples (Mactung North pluton and Mactung South pluton) and three argillite samples (Unit 1). Further details about the samples are presented in the *Online Resource 1*.

Scheelite from Cantung include two samples from an early stage quartz vein cutting across the Mine stock pluton, two samples from argillite units (Lower Argillite and Upper Argillite), one sample from the garnet-pyroxene skarn (hosted in the Ore Limestone), one sample from the pyroxene skarn (hosted in the Swiss-Cheese Limestone), one sample from the amphibole-rich facies (hosted in the Swiss-Cheese Limestone) and one sample from the biotite-rich facies (hosted in the Ore Limestone). Scheelite from Mactung include one sample from argillite (hosted in Unit 1), one sample from the garnet-

pyroxene skarn (hosted in Unit 3E), one sample from the pyroxene skarn (hosted in Unit 3E) and one sample from the amphibole-rich facies (hosted in Unit 3F).

## ❑ APPENDIX S3: DETAILED METHODS

### ➤ Whole rock composition

The mineralogy and mineral zonation of samples was determined in thin sections through transmitted and reflected light microscopy and Scanning Electron Microscopy (SEM). Unaltered samples were selected for whole rock analyses and ground in a shatter box using an alumina mill.

Whole rock Samarium-Neodymium isotope compositions were determined through mass spectrometry of Sm and Nd fractions separated and measured at the Crustal Re-Os Geochronology Laboratory and CCIM ICPMS facilities at the University of Alberta. Sample powders were weighed and spiked with a known amount of mixed  $^{150}\text{Nd}$ - $^{149}\text{Sm}$  tracer solution calibrated directly against the Caltech mixed Sm/Nd normal described by Wasserburg et al. (1981). Samarium and neodymium fractions were separated following the procedures described in Creaser et al. (1997) and Unterschutz et al. (2002).

The purified Sm and Nd fractions were analyzed for isotopic composition and concentration using a Nu Plasma™ multi-collector inductively coupled plasma mass spectrometer (MC-ICP-MS) at CCIM-ICPMS facility at the University of Alberta. All Nd isotope ratios were normalized for variable mass fractionation to a value of  $^{146}\text{Nd} / ^{144}\text{Nd} = 0.7219$  using the exponential fractionation law. The  $^{143}\text{Nd} / ^{144}\text{Nd}$  ratios presented here are relative to a value of 0.511850 for the La Jolla Nd isotopic standard, monitored by use of an in-house Alfa Nd isotopic standard. The value of  $^{143}\text{Nd} / ^{144}\text{Nd}$  obtained for the JNdi-1 standard following this procedure was  $0.512109 \pm 8$  (2SE) compared to a known value  $0.512107 \pm 7$  (Tanaka et al., 2000). Sm isotopic abundances were normalized for variable mass fractionation to a value of 1.17537 for  $^{152}\text{Sm} / ^{154}\text{Sm}$  also using the exponential law. The Nd isotope standard “Shin Etsu: J-Ndi-1” (Tanaka et al., 2000) was also analyzed using the same procedures. Using the mixed  $^{150}\text{Nd}$ - $^{149}\text{Sm}$  tracer, the measured  $^{147}\text{Sm} / ^{144}\text{Nd}$  ratios for the synthetic BCR-1 standard range from 0.1380 to 0.1382, suggesting reproducibility for  $^{147}\text{Sm} / ^{144}\text{Nd}$  of  $\sim \pm 0.1\%$  for real rock powders.

### ➤ Scheelite composition

Chemical homogeneity/heterogeneity in scheelite was tested in thin section through cathodoluminescence imaging at the Scanning Electron Microscope Laboratory at the University of Alberta using a Zeiss EVO LS15 Scanning Electron Microscope and

through point mode LA-ICPMS transects perpendicular to growth zones in individual grains.

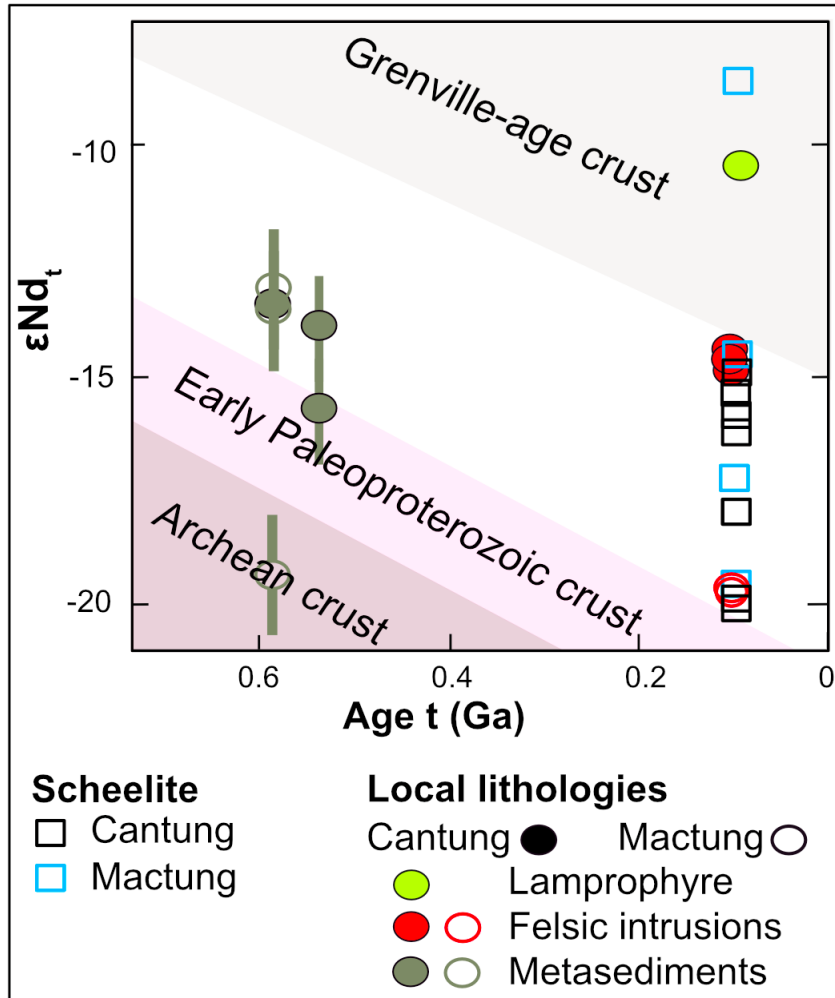
The Samarium-Neodymium isotope compositions of scheelite were determined through solution MC-ICPMS of scheelite separates and through in-situ laser ablation split stream analyses (LASS) ICPMS of thin sections and grain mounts. These two procedures were combined to (1) verify the accuracy of the results and (2) to evaluate compositions in samples where the concentrations of Sm or Nd were too low to obtain meaningful results through LASS.

For solution MC-ICPMS, scheelite grains were separated at the SELFRAG laboratory of the Canadian Centre for Isotopic Microanalysis (CCIM) at the University of Alberta, then handpicked under a binocular microscope under ultraviolet light. Scheelite powders were obtained using an agate mortar. Scheelite dissolution and Sm and Nd fractions separation were performed at the Crustal Re-Os Geochronology Laboratory of the University of Alberta following procedures described by Kempe et al. (2001).

Only four scheelite samples were analyzed via LASS ICP MS: one sample from the Mactung pyroxene skarn, one from the Cantung quartz vein, one from Mactung argillites and one from Cantung argillites. Simultaneous Sm-Nd isotope and trace element (Sm and Nd) measurements were carried out in the Arctic Resources Laboratory at the University of Alberta (Luo et al., 2019). The scheelite samples were ablated using the LASS technique (Yuan et al., 2008; Xie et al. 2008; Fisher et al., 2014). Samples were ablated using a 193 nm Resolution Excimer ArF laser equipped with a Laurin-technic S-155 two-volume ablation cell. Analyses were performed using a laser fluence of 6 J/cm<sup>2</sup> and a repetition rate of 10 Hz. Analysis time consisted of 60 seconds of background followed by 70 seconds of ablation and then 40 seconds of sample washout. The carrier gas was a mixture of ~1.6 L/min Ar and 14 ml/min N<sub>2</sub>, which entered tangentially from the top of the S-155 ablation cell funnel and ~800 ml/min He entering from the side of the cell. This yielded a pressure in the ablation cell of ~7.5 KPa. The ablated sample aerosol, He, N<sub>2</sub> and Ar mixture was then split after the laser cell using a Y-piece, diverting the ablation product to a Thermo Neptune Plus using multiple Faraday detectors with 1011 Ω amplifiers operating in static collection mode (for Sm-Nd) and a Thermo Element-XR 2 mass spectrometer using a single secondary electron multiplier detector in peak hopping mode (for trace elements). The length of tubing was equalized such that the ablated sample aerosol arrives simultaneously at both mass spectrometers. Calibration was performed using NIST SRM 612 in conjunction with internal standardization using isotope <sup>43</sup>Ca. The results of the measurements of secondary standards (e.g., NIST614) agree with the reference values within relative uncertainties of typically 5–10% or better at the 95% confidence level.

The present-day CHUR values used for the initial  $\epsilon\text{Nd}$  ( $\epsilon\text{Nd}_i$ ) calculation are  $^{143}\text{Nd}/^{144}\text{Nd}=0.512638$  and  $^{147}\text{Sm}/^{144}\text{Nd}=0.1967$ .

□ APPENDIX S4: DETAILS FOR DATA PRESENTED IN FIGURES



Supplementary Figure S1.  $\epsilon\text{Nd}$  at time of formation ( $t$ ) for scheelite, and local lithologies in the Canadian Tungsten Belt (Blow-up of Figure 3, focusing on data acquired in this study). Squares and circles are data acquired in this study with squares representing Nd isotopic compositions of scheelite and circles representing neodymium isotopic compositions of local lithologies associated with the Cantung and Mactung deposits.

➤ **Data presented in Figure 1:**

1/Basement rocks and faults are from Whitmeyer and Karlstrom (2007) (<2.0 Ga orogens and arcs, 1.9-1.8 Ga reworked Archean crust, and >2.5 Ga Archean crust) and from Esteve et al. (2020) (Mackenzie craton and Canadian shield).

2/ $\epsilon$ Nd data are from Morris and Creaser (2008) for the Canadian Cordillera and from Chapman et al. (2017) for the US Cordillera.

3/Tungsten deposits and classification are from Sinclair et al. (2011) and Sinclair et al. (2014).

➤ **Compiled data presented in Figure 3:**

Archean and Early Proterozoic crust fields are from Villeneuve et al. (1993), Grenville-age crust field is from Garzione et al. (1997) and references therein. The source data from Figure 3 are presented in the *Online Resource 1*.

- ***Igneous / meta-igneous units:***

1/Lamprophyre data include: lamprophyres from the Scheelite Dome (Mair et al., 2011), from near the Roy pluton, near the Pelly River pluton, and from the Cantung deposit (Rasmussen, 2013);

2/ Felsic (meta-)igneous rocks data include: Bonnet Plume River intrusions (Northeastern Yukon) (Thorkelson et al., 2001), Fort Simpson magnetic High intrusions (Northeastern BC & Southern Yukon) (Villeneuve et al., 1991), and intrusions and orthogneiss from the Taltson, Buffalo Head, Chinchaga and Ksituan domains (Northern Alberta) (Theriault and Ross, 1991);

3/ Mafic (meta-)igneous rocks data include: Archean/Early Proterozoic metagabbro from the Buffalo Head domain (Northern Alberta) (Theriault and Ross, 1991), Neoproterozoic basalts/sills from Little Dal basalts and Tsezotene sills (Mackenzie Mtns, NWT) (Dudas and Lustwerk, 1997), and recent to Tertiary basalts from the Iskut-Unuk rivers volcanic field (SW Yukon) (Cousens and Bevier, 1995), from Watson Lake (Abraham et al., 2001), and from the Mount Skukum Volcanic Complex and the Bennett Lake Volcanic Complex (Morris and Creaser, 2003).

- ***Sedimentary / meta-sedimentary units:***

1/ Paleozoic metasediments data include data from Garzione et al. (1997) (Yukon and Northwest Territories) and from Cousens (2007) (Eastern Yukon);

2/ Windermere Supergroup (Yukon and NWT) data are from Garzzone et al. (1997);

3/Mackenzie Mountains Supergroup (NWT) data are from Rainbird et al. (1997);

4/Wernecke Supergroup (Yukon) data are from Thorkelson et al. (2005).

➤ **Data from this study presented in Figure 3 and in Supplementary Figure 1:**

Detailed data for this study are presented in the *Online Resource 1*.

- ***Scheelite data***

Scheelite from Cantung are from the garnet-pyroxene skarn, the pyroxene skarn, the amphibole-rich facies, the biotite-rich facies, argillite, and a quartz vein in Mine Stock pluton.

Scheelite from Mactung are from the garnet-pyroxene skarn, the pyroxene skarn, the amphibole-rich facies, and argillite.

Details about these different facies can be found in Elongo et al. (2020).

- ***Whole rock data:***

1/ Lamprophyre: Cretaceous lamprophyre from the Cantung deposit;

2/ Felsic intrusions data include data from the Cretaceous Mine Stock pluton and aplite from Cantung, and from the Cretaceous Mactung North and South plutons;

3/ Metasediments data include data from the Cambrian Swiss-Cheese limestone and argillites from Cantung and the Cambrian argillites from Mactung.

➤ **Data presented in Figure 4:**

The source data from Figure 4 are presented in the *Online Resource 2*.

The oxidation state of the plutons was assessed based on the  $\log_{10}(\text{Fe}_2\text{O}_3/\text{FeO})$  vs  $\text{FeO}_{\text{total}}$  classification scheme from Blevin (2004). Iron oxides and zircon saturation temperatures (ZST) data are taken from Rasmussen (2013) (NWT and Yukon, Canada), Hart et al. (2004), Bateman et al. (1965) and Chapman et al. (2021) (Western USA and Mexico). Chapman et al. (2021) data are a compilation of data from G. Haxel (unpublished), Shaw and Guilbert (1990), Force (1997), Keith and Reynolds (1980), Best et al. (1974), Lee et al. (1981), Lee and Van Loenen (1971), and from John and Wooden (1990).

Some units/plutons compiled by Chapman et al. (2021) are represented by several samples with different iron oxides content and different ZST. For these units/plutons, samples with the same oxidation state were lumped together and an average ZST was given for each oxidation state. For each of these units/plutons, the percentage represented

by samples with the same oxidation state is also given and presented as a partitioned circle in Figure 4.

Zircon saturation temperatures (Watson and Harrison, 1983) presented in these studies are calculated from whole rock compositions based on the concentrations of zirconium, silica, aluminum and alkalis in the rock.

Zircon solubility is a function of temperature and composition of melt as defined by the following equation:

$$\ln D^{\text{Zr,zircon/melt}} = \{-3.8 - [0.85(M-1)]\} + 12900/T \quad (\text{Watson and Harrison, 1983})$$

where  $D^{\text{Zr,zircon/melt}}$  is the ratio of Zr concentration in zircon (~496000 ppm) to that in the melt, M is the cation ratio  $(\text{Na}+\text{K}+2\cdot\text{Ca})/(\text{Al}\cdot\text{Si})$  accounting for dependence of zircon solubility on  $\text{SiO}_2$  and peraluminosity of the melt (Miller et al., 2003), and T is the temperature (Kelvins). Rearranging the equation to yield T provides the zircon saturation temperature geothermometer equation:  $T_{\text{Zr}}=12900/[2.95 + 0.85M + \ln(496000/\text{Zr}_{\text{melt}})]$ . Zircon saturation temperatures can be used to estimate initial melt temperatures; however, these estimates are influenced by the inherited zircon content of the melt (Miller et al., 2003). The zircon saturation temperature geothermometer provides a good estimate of initial magma temperature at the source for plutons with abundant inherited zircon and provides an underestimate initial temperature for plutons poor in inherited zircon (Miller et al., 2003). Thus, it provides minimum estimates of initial temperature if the magma was undersaturated, but maximum estimates of initial temperature if the magma was saturated (Miller et al., 2003).

## REFERENCES

- Abraham, A. C., Francis, D., & Polvé, M. (2001). Recent alkaline basalts as probes of the lithospheric mantle roots of the northern Canadian Cordillera. *Chemical Geology*, 175(3-4), 361-386.
- Atkinson, D., & Baker, D.J. (1986). Recent developments in the geologic understanding of Mactung. *Mineral Deposits of the Northern Cordillera*. *Canad. Inst. Mining Metal.*, 37, 234-244.
- Bateman, P. C., Pakiser, L. C., & Kane, M. F. (1965). *Geology and tungsten mineralization of the Bishop district, California, with a section on gravity study of Owens Valley and a section on seismic profile* (No. 470). US Govt. Print. Off.,
- Best, M. G., & Brimhall, W. H. (1974). Late Cenozoic alkalic basaltic magmas in the western Colorado Plateaus and the Basin and Range transition zone, USA, and their bearing on mantle dynamics. *Geological Society of America Bulletin*, 85(11), 1677-1690.

- Blevin, P. L. (2004). Redox and compositional parameters for interpreting the granitoid metallogeny of eastern Australia: Implications for gold-rich ore systems. *Resource Geology*, 54(3), 241-252.
- Blusson, S. L. (1968). Geology and tungsten deposits near the headwaters of Flat River, Yukon Territory and southwestern district of Mackenzie, Canada (Vol. 67, No. 22). Department of Energy, Mines and Resources
- Chapman, J. B., Ducea, M. N., Kapp, P., Gehrels, G. E., & DeCelles, P. G. (2017). Spatial and temporal radiogenic isotopic trends of magmatism in Cordilleran orogens. *Gondwana Research*, 48, 189-204.
- Chapman, J. B., Runyon, S. E., Shields, J., Lawler, B. L., Pridmore, C. J., Scoggin, S. H., ... & Haxel, G. B. (2021). The North American Cordilleran Anatectic Belt. *Earth-Science*
- Cousens, B. L. (2007). Radiogenic isotope studies of Pb-Zn mineralization in the Howards Pass area, Selwyn Basin. *Mineral and Energy Resource Potential of the Proposed Expansion to the Nahanni National Park Reserve, North Cordillera, Northwest Territories: Geological Survey of Canada, Open File, 5344*, 14.
- Cousens, B. L., & Bevier, M. L. (1995). Discerning asthenospheric, lithospheric, and crustal influences on the geochemistry of Quaternary basalts from the Iskut–Unuk rivers area, northwestern British Columbia. *Canadian Journal of Earth Sciences*, 32(9), 1451-1461.
- Creaser, R. A., Erdmer, P., Stevens, R. A., & Grant, S. L. (1997). Tectonic affinity of Nisutlin and Anvil assemblage strata from the Teslin tectonic zone, northern Canadian Cordillera: Constraints from neodymium isotope and geochemical evidence. *Tectonics*, 16(1), 107-121.
- Dick, L. A., & Hodgson, C. J. (1982). The MacTung W-Cu (Zn) contact metasomatic and related deposits of the northeastern Canadian Cordillera. *Economic Geology*, 77(4), 845-867.
- Dudás, F. Ö., & Lustwerk, R. L. (1997). Geochemistry of the Little Dal basalts: continental tholeiites from the Mackenzie Mountains, Northwest Territories, Canada. *Canadian Journal of Earth Sciences*, 34(1), 50-58.
- Elongo, V., Lecumberri-Sanchez, P., Legros, H., Falck, H., Adlakha, E., Roy-Garand, A., n.d. Paragenetic constraints on the Cantung, Mactung and Lened tungsten skarn deposits, Canada: implications for grade distribution. *Ore Geol. Rev.*
- Estève, C., Audet, P., Schaeffer, A. J., Schutt, D. L., Aster, R. C., & Cubley, J. F. (2020). Seismic evidence for craton chiseling and displacement of lithospheric mantle by the Tintina fault in the northern Canadian Cordillera. *Geology*, 48(11), 1120-1125.

- Fischer, B.J., Martel, E., and Falck, H., (2018). Geology of the Mactung tungsten skarn and area – Review and 2016 field observations; Northwest Territories Geological Survey, NWT Open File 2018-02, 84 pages and appendices.
- Fisher, C. M., Vervoort, J. D., & DuFrane, S. A. (2014). Accurate Hf isotope determinations of complex zircons using the “laser ablation split stream” method. *Geochemistry, Geophysics, Geosystems*, 15(1), 121-139.
- Force, E. R. (1997). Geology and mineral resources of the Santa Catalina Mountains, southeastern Arizona: A cross-sectional approach.
- Garzzone, C. N., Patchett, P. J., Ross, G. M., & Nelson, J. (1997). Provenance of Paleozoic sedimentary rocks in the Canadian Cordilleran miogeocline: a Nd isotopic study. *Canadian Journal of Earth Sciences*, 34(12), 1603-1618.
- Gebru, A. L. (2017). Petrogenesis of Granitoids in the Vicinity of the Mactung Tungsten Skarn Deposit, NE Yukon-Northwest Territories: Characterization of Skarn Mineralization and Causative Plutons through Geological, Petrochemical, Mineralogical, and Geochronological Analysis. UnPub PhD Thesis, University of New Brunswick, New Brunswick, Canada.
- Gordey, S. P., & Anderson, R. G. (1993). Evolution of the northern Cordilleran miogeocline, Nahanni map area (105I), Yukon and Northwest Territories. *Geol. Surv. Canada Mem.*, 428, 214p.
- Hart, C. J., Mair, J. L., Goldfarb, R. J., & Groves, D. I. (2004). Source and redox controls on metallogenic variations in intrusion-related ore systems, Tombstone-Tungsten Belt, Yukon Territory, Canada. *Earth and Environmental Science Transactions of The Royal Society of Edinburgh*, 95(1-2), 339-356.
- John, B. E., & Wooden, J. (1990). Petrology and geochemistry of the metaluminous to peraluminous Chemehuevi Mountains Plutonic Suite, southeastern California. *The Nature and Origin of Cordilleran Magmatism. Geological Society of America, Memoir*, 174, 71-98.
- Keith, S. B., & Reynolds, S. J. (1980). Geochemistry of Cordilleran metamorphic core complexes. Cordilleran metamorphic core complexes and their uranium favorability: US Department of Energy Open-File Report GJBX-256 (80), 321.
- Kempe, U., Belyatsky, B., Krymsky, R., Kremenetsky, A., & Ivanov, P. (2001). Sm–Nd and Sr isotope systematics of scheelite from the giant Au (–W) deposit Muruntau (Uzbekistan): implications for the age and sources of Au mineralization. *Mineralium Deposita*, 36(5), 379-392.
- Lee, D. E., & Van Loenen, R. E. (1971). *Hybrid granitoid rocks of the southern Snake Range, Nevada* (pp. 1-46). US Government Printing Office.

- Lee, D. E., Kistler, R. W., Friedman, I., & Van Loenen, R. E. (1981). Two-mica granites of northeastern Nevada. *Journal of Geophysical Research: Solid Earth*, 86(B11), 10607-10616.
- Lentz, C. (2020). Genesis of Gold Mineralization at the Cantung W-Cu skarn deposit, N.W.T. UnPub MSc Thesis, University of New Brunswick, New Brunswick, Canada.
- Luo, Y., Pearson, D.G., Scott, J., Palmer, M.C., Fisher, C.M., Sarkar, C., Vezinet, A., Lecumberri-Sanchez, P., 2019. Simultaneous In situ Analysis of Sm-Nd isotopes and Trace Elements in Scheelite by Laser Ablation Split Stream ICP-MS: Challenges and Emerging Approaches., 2019 North America laser ablation workshop, Austin, p. 34.
- Mair, J. L., Farmer, G. L., Groves, D. I., Hart, C. J., & Goldfarb, R. J. (2011). Petrogenesis of postcollisional magmatism at Scheelite Dome, Yukon, Canada: evidence for a lithospheric mantle source for magmas associated with intrusion-related gold systems. *Economic Geology*, 106(3), 451-480.
- Mathieson, G. A., & Clark, A. H. (1984). The Cantung E Zone scheelite skarn orebody, Tungsten, Northwest Territories; a revised genetic model. *Economic Geology*, 79(5), 883-901.
- Miller, C. F., McDowell, S. M., & Mapes, R. W. (2003). Hot and cold granites? Implications of zircon saturation temperatures and preservation of inheritance. *Geology*, 31(6), 529-532.
- Morris, G. A., & Creaser, R. A. (2008). Correlation of mid-Cretaceous granites with source terranes in the northern Canadian Cordillera. *Canadian Journal of Earth Sciences*, 45(3), 389-403.
- Morris, G. A., & Creaser, R. A. (2003). Crustal recycling during subduction at the Eocene Cordilleran margin of North America: a petrogenetic study from the southwestern Yukon. *Canadian Journal of Earth Sciences*, 40(12), 1805-1821.
- Rainbird, R. H., McNicoll, V. J., Theriault, R. J., Heaman, L. M., Abbott, J. G., Long, D. G. F., & Thorkelson, D. J. (1997). Pan-continental river system draining Grenville Orogen recorded by U-Pb and Sm-Nd geochronology of Neoproterozoic quartzarenites and mudrocks, northwestern Canada. *The Journal of Geology*, 105(1), 1-17.
- Rasmussen, K. L., Lentz, D. R., Falck, H., & Pattison, D. R. (2011). Felsic magmatic phases and the role of late-stage aplitic dykes in the formation of the world-class Cantung Tungsten skarn deposit, Northwest Territories, Canada. *Ore Geology Reviews*, 41(1), 75-111.

- Rasmussen, K.L. (2013) The timing, composition, and petrogenesis of syn- to post-accretionary magmatism in the northern Cordilleran miogeocline, eastern Yukon and southwestern Northwest Territories. Ph.D. Thesis, University of British Columbia, Vancouver, British Columbia, Canada, 788 pp.
- Selby, D., Creaser, R. A., Heaman, L. M., & Hart, C. J. (2003). Re-Os and U-Pb geochronology of the Clear Creek, Dublin Gulch, and Mactung deposits, Tombstone Gold Belt, Yukon, Canada: absolute timing relationships between plutonism and mineralization. *Canadian Journal of Earth Sciences*, 40(12), 1839-1852.
- Shaw, A. L., & Guilbert, J. M. (1990). Geochemistry and metallogeny of Arizona peraluminous granitoids with reference to Appalachian and European occurrences. *Ore-bearing granite systems: petrogenesis and mineralizing processes, Geol Soc Am Spec Paper*, 246, 317-356.
- Sinclair, W D; Gonevchuk, G A; Korostelev, P G; Semenyak, B I; Rodionov, S; Seltmann, R; Stemprok, M. (2011). World distribution of tin and tungsten deposits. Geological Survey of Canada, Open File 5482, <https://doi.org/10.4095/287906>
- Sinclair, W D; Gonevchuk, G A; Korostelev, P G; Semenyak, B I; Rodionov, S M; Seltmann, R; Stemprok, M. (2014). Geological Survey of Canada, Open File 7688, <https://doi.org/10.4095/295581>
- Tanaka, T., Togashi, S., Kamioka, H., Amakawa, H., Kagami, H., Hamamoto, T., ... & Kunimaru, T. (2000). JNdi-1: a neodymium isotopic reference in consistency with LaJolla neodymium. *Chemical Geology*, 168(3-4), 279-281.
- Thériault, R. J., & Ross, G. M. (1991). Nd isotopic evidence for crustal recycling in the ca. 2.0 Ga subsurface of western Canada. *Canadian Journal of Earth Sciences*, 28(8), 1140-1147.
- Thorkelson, D. J., Abbott, J. G., Mortensen, J. K., Creaser, R. A., Villeneuve, M. E., McNicoll, V. J., & Layer, P. W. (2005). Early and middle Proterozoic evolution of Yukon, Canada. *Canadian Journal of Earth Sciences*, 42(6), 1045-1071.
- Thorkelson, D. J., Mortensen, J. K., Creaser, R. A., Davidson, G. J., & Abbott, J. G. (2001). Early Proterozoic magmatism in Yukon, Canada: constraints on the evolution of northwestern Laurentia. *Canadian Journal of Earth Sciences*, 38(10), 1479-1494.
- Unterschutz, J. L., Creaser, R. A., Erdmer, P., Thompson, R. I., & Daughtry, K. L. (2002). North American margin origin of Quesnel terrane strata in the southern Canadian Cordillera: Inferences from geochemical and Nd isotopic characteristics of Triassic metasedimentary rocks. *Geological Society of America Bulletin*, 114(4), 462-475.

- Villeneuve, M. E. (1993). *Tectonic subdivision and U-Pb geochronology of the crystalline basement of the Alberta Basin, Western Canada* (Vol. 447). Geological Survey of Canada.
- Villeneuve, M. E., Thériault, R. J., & Ross, G. M. (1991). U–Pb ages and Sm–Nd signature of two subsurface granites from the Fort Simpson magnetic high, northwest Canada. *Canadian Journal of Earth Sciences*, 28(7), 1003-1008.
- Wasserburg, G. J., Jacobsen, S. B., DePaolo, D. J., McCulloch, M. T., & Wen, T. (1981). Precise determination of SmNd ratios, Sm and Nd isotopic abundances in standard solutions. *Geochimica et Cosmochimica Acta*, 45(12), 2311-2323.
- Watson, E. B., & Harrison, T. M. (1983). Zircon saturation revisited: temperature and composition effects in a variety of crustal magma types. *earth and planetary science letters*, 64(2), 295-304.
- Whitmeyer, S. J., & Karlstrom, K. E. (2007). Tectonic model for the Proterozoic growth of North America. *Geosphere*, 3(4), 220-259.
- Xie, L., Zhang, Y., Zhang, H., Sun, J., & Wu, F. (2008). In situ simultaneous determination of trace elements, U-Pb and Lu-Hf isotopes in zircon and baddeleyite. *Chinese Science Bulletin*, 53(10), 1565-1573.
- Yuan, H. L., Gao, S., Dai, M. N., Zong, C. L., Günther, D., Fontaine, G. H., ... & Diwu, C. (2008). Simultaneous determinations of U–Pb age, Hf isotopes and trace element compositions of zircon by excimer laser-ablation quadrupole and multiple-collector ICP-MS. *Chemical Geology*, 247(1-2), 100-118.